

## Plastic deformation of single crystals of Pt<sub>3</sub>Al with the L1<sub>2</sub> structure

Norihiko L. Okamoto, Yoshihiko Hasegawa, Wataro Hashimoto, and Haruyuki Inui

*Department of Materials Science and Engineering, Kyoto University, Kyoto 606-8501, Japan*

Corresponding author:

Norihiko L. Okamoto

Department of Materials Science and Engineering, Kyoto University

Sakyo-ku, Kyoto 606-8501, Japan

Tel: +81-75-753-5481

Fax: +81-75-753-5461

Email: n.okamoto@at4.ecs.kyoto-u.ac.jp

### Abstract

The plastic deformation behaviour of single crystals of Pt<sub>3</sub>Al with the L1<sub>2</sub> structure having an off-stoichiometric composition of Pt-27at.%Al has been investigated in compression from 77 to 1073 K. The L1<sub>2</sub> structure is not stable below around 220 K, transforming into either D0c or D0c' structure. Slip occurs along  $\langle 110 \rangle$  both on (001) and on (111) with slip on (001) being the primary slip system, which operates for most crystal orientations except for near [001], accompanied by a considerably lower CRSS (critical resolved shear stress). The CRSS tends to decrease gradually with increasing temperature for both slip in the temperature range where the L1<sub>2</sub> phase is stable, except for a moderate increase in CRSS observed above 673 K for slip on (001). Dislocations with  $\mathbf{b} = [\bar{1}01]$  dissociate into two collinear superpartials with  $\mathbf{b} = 1/2[\bar{1}01]$  separated by an APB on the corresponding slip plane for both slip on (001) and (111). For slip on (111), dislocations tend to align along their screw orientation at room temperature, suggesting the high Peierls stress for their motion. The possibility of showing the normal (large negative) temperature dependence of CRSS at low temperatures as well as the reason for the absence of the anomalous (positive) temperature dependence of CRSS for slip on (111) at high temperatures is discussed.

Keywords: intermetallic compound; Pt<sub>3</sub>Al; compression deformation behaviour; dislocation; transmission electron microscopy

## 1. Introduction

Intermetallic compounds with the  $L1_2$  structure have been extensively investigated over the last three or four decades as one of the most valuable intermetallic compounds, due to their technological importance as the strengthening phase in heat-resistant Ni-based superalloys. Many excellent review papers, such as that by Veyssi re and Saada [1], have been published, promoting our understanding of the mechanical properties of  $L1_2$  compounds on the basis of dislocation mechanisms [1-4]. Extensive studies have concentrated on those  $L1_2$  compounds that exhibit an anomalous positive temperature dependence of yield stress at high temperatures.  $Ni_3Al$  is usually cited as the representative  $L1_2$  compound in this category, although many other  $L1_2$  compounds, such as  $Ni_3Si$ ,  $Ni_3Ge$ ,  $Co_3Ti$  and so on, are known to exhibit a similar anomalous temperature dependence of yield stress [1-4]. However, there are some other  $L1_2$  compounds that do not exhibit the anomalous positive temperature dependence of yield stress [6-9]. Many are known instead to exhibit a large negative temperature dependence of yield stress at low temperatures.  $Pt_3Al$  is usually cited as the representative  $L1_2$  compound for this second category. According to Vitek and co-workers [4,10-14], the difference in the temperature dependence of yield stress for the two categories of  $L1_2$  compounds can be explained in terms of the dissociation scheme of the dislocation with  $\mathbf{b}$  (Burgers vector) =  $\langle 110 \rangle$  and the planarity of the core structure of the resultant partial dislocation. For those  $L1_2$  compounds that exhibit a yield stress anomaly (such as  $Ni_3Al$ ), the dislocation with  $\mathbf{b} = \langle 110 \rangle$  is believed to dissociate into two collinear superpartial dislocations with  $\mathbf{b} = 1/2\langle 110 \rangle$  separated by an APB (anti-phase boundary). The core of each of the APB-coupled superpartial dislocations is believed to be planar and hence glissile [10-14]. The yield stress anomaly is generally believed to be caused by the thermally activated cross-slip of these APB-coupled dislocations from the (111) octahedral to (010) cube planes. The cross-slip is believed to be driven by anisotropy in the APB energy on (111) ( $\gamma_{APB}^{(111)}$ ) and that on (001) ( $\gamma_{APB}^{(001)}$ ) [13,15] and a torque force acting between screw APB-coupled superpartial pair [16]. For those  $L1_2$  compounds that exhibit a large negative temperature dependence of yield stress at low temperatures (such as  $Pt_3Al$ ), on the other hand, the dislocation with  $\mathbf{b} = \langle 110 \rangle$  is believed to dissociate into two superpartial dislocations with  $\mathbf{b} = 1/3\langle 112 \rangle$  separated by an SISF (superlattice intrinsic stacking fault). The core of the SISF-coupled superpartial dislocation is believed to be non-planar, at least along the screw orientation and, hence, sessile [4, 10-12,14]. Then, the Peierls stress for the motion is expected to be high and, since thermal activation is needed for the motion, the yield stress is considered to strongly depend on temperature

at low temperatures. Which of the two dissociation schemes (either of the APB-type or SISF-type) is preferred is considered to be determined by the relative magnitudes of the APB energy on (111) and the SISF energy on (111) ( $\gamma_{SISF}^{(111)}$ ). The dissociation of the SISF-type is preferred as the relative stability of SISF is increased (i.e., with lower SISF energies) so that the condition of  $\ln(8\pi \gamma_{SISF}^{(111)}/c_{44}a_0) < 2\ln(4\pi \gamma_{APB}^{(111)}/c_{44}a_0)+1$  is satisfied [10]. Pt<sub>3</sub>Al is assumed to satisfy this condition with a low SISF energy [4,10,11,14], although some first-principles calculations indicate that the SISF energy is not as small as that to satisfy the above condition in Pt<sub>3</sub>Al [17,18].

The deformation behaviour of Pt<sub>3</sub>Al was investigated experimentally both in poly- [5,6,9] and in single-crystalline [7,8] forms. Slip is reported to occur on both (111) and (001), and the CRSS (critical resolved shear stress) for both slip decreases rapidly with increasing temperature at low temperatures [7,8]. However, since no TEM study was made on the dislocation structures, nothing is known about the dislocation mechanism including the dissociation schemes for the large negative temperature dependence for yield stress at low temperatures. On top of that, none of the fundamental materials constants, such as planar fault energies and elastic constants that are needed to further understand the deformation behaviour, has been experimentally determined yet for Pt<sub>3</sub>Al. Some theoretical calculations based on first-principles methods have raised a serious question about the phase stability of the L1<sub>2</sub> structure as the ground state of Pt<sub>3</sub>Al with the stoichiometric composition [18,19]. The instability of the L1<sub>2</sub> structure as the ground state of Pt<sub>3</sub>Al is consistent with some experimental results which showed that the L1<sub>2</sub> structure is only stable at high temperatures at the stoichiometric composition and that the L1<sub>2</sub> to tetragonal D0c phase transformation occurs at low temperature with the transformation temperature decreasing with the increase in the Al concentration in the Al-rich concentrations [20,21]. However, it is unclear as yet whether or not the deformation behaviour of single crystals of Pt<sub>3</sub>Al as reported by Wee et al. [7] and Heredia et al. [8] was affected by the possible instability of the L1<sub>2</sub> structure of Pt<sub>3</sub>Al at low temperatures.

In the present study, we investigate the plastic deformation behaviour of single crystals of Pt<sub>3</sub>Al with an off-stoichiometric composition (Pt-27at.%Al), exactly the same as that used by Wee et al. [7] and Heredia et al. [8]. We examine the phase stability of the L1<sub>2</sub> phase to see how the deformation behaviour is affected by the phase stability, especially at low temperatures. We determine the single-crystal elastic constants of Pt<sub>3</sub>Al for the first time. We also examine the dislocation structures after

compression deformation made at various temperatures to elucidate not only the dislocation mechanisms that account for the observed temperature dependence of yield stress but also planar fault energies. We finally discuss the observed deformation behaviour of Pt<sub>3</sub>Al in the light of some fundamental materials constants such as planar fault energies and elastic constants determined in the present study.

## 2. Experimental procedures

Ingots with a nominal composition of Pt-27 at% Al were prepared by arc-melting high-purity Pt and Al under an Ar gas flow. Single crystals of Pt<sub>3</sub>Al were grown from these ingots by the Bridgman method with an alumina crucible. After determining the crystallographic orientations by the X-ray back reflection Laue method, specimens were cut from the crystal by spark-machining and mechanically polished with SiC paper and then with diamond paste.

Measurements of thermal expansion were carried out with a push-rod type differential dilatometer (Shimadzu TMA50) in the temperature range from 89 K to room temperature at a heating rate of 10 K/min. Measurements of elastic constants were carried out by the rectangular parallelepiped resonance (RPR) method [22] at room temperature. Compression tests were conducted on an Instron-type testing machine from liquid nitrogen temperature to 1073 K at a strain rate of 10<sup>-4</sup> s<sup>-1</sup>. Compression tests at low temperatures were performed with a specimen immersed in liquid nitrogen (77 K), while tests above room temperature were carried out *in vacuo*. The compression axis orientations investigated were [001], [ $\bar{1}$  2 12], [ $\bar{1}$ 26] and [ $\bar{2}$  34], as shown in Fig. 1. The specimen size was 1.5 × 1.5 × 4.5 mm<sup>3</sup>. Operative slip planes were determined by slip trace analysis on two orthogonal surfaces by optical microscopy. Dislocation structures were examined with a JEM-2000FX TEM operated at 200 kV. Selected-area electron diffraction (SAED) patterns were taken using a cryo-TEM stage (Gatan, HCHDT-3010) in the temperature range from 80 K to room temperature, to detect a possible phase transformation. Thin foils for TEM observations were cut parallel to the macroscopic slip plane (either (111) or (001)) and were subjected to ion milling with 4 keV Ar ions for perforation.

## 3. Experimental Results

### 3.1. Stability of the L1<sub>2</sub> phase

SAED patterns of Pt<sub>3</sub>Al with the composition of Pt-27at.%Al taken along some low-indexed ([001], [110] and [111]) incident directions are shown in Figs. 2(a)-(c), respectively. All these SAED patterns are consistently indexed as those from the L1<sub>2</sub>

structure. This confirms that the  $L1_2$  structure is stable at room temperature (and above) for the composition of Pt-27at.%Al. On the other hand, the  $L1_2$  structure is not stable for  $Pt_3Al$  with the stoichiometric composition of Pt-25at.%Al, even at room temperature, as is evident from the occurrence of additional diffraction spots in the corresponding SAED patterns (Figs. 2(d)-(f)). These SAED patterns are indexed as those from the  $Pt_3Ga$  structure\* ( $tP16$ ,  $P4/mbm$ ). This is consistent with the result of first principles calculation by Chauke et al [19] who showed that the ground state of stoichiometric  $Pt_3Al$  is the  $Pt_3Ga$  structure but not the  $L1_2$  structure.

Since the  $L1_2$  phase of  $Pt_3Al$  is reported to transform to tetragonal  $D0c$  ( $U_3Si$ ,  $tI16$ ,  $I4/mcm$ ) and  $D0c'$  ( $Ir_3Si$ ,  $tI16$ ,  $I4/mcm$ ) phases at low temperatures [20,21], the thermal stability of the  $L1_2$  structure of Pt-27at.%Al was investigated by the measurement of thermal expansion and the inspection of SAED patterns at low temperatures. Thermal expansion of  $Pt_3Al$  with the composition of Pt-27at.%Al measured below room temperature is plotted in Fig. 3 as relative elongation with respect to the original specimen length at 89 K. On heating, a discontinuous increase occurs at around 220 K in the relative elongation versus temperature curve, indicating the occurrence of phase transformation. The value of coefficient for thermal expansion (CTE) of  $Pt_3Al$  estimated in the temperature range where the  $L1_2$  phase is stable is  $10.1 \times 10^{-6} K^{-1}$ , which is a little smaller than those ( $13-16 \times 10^{-6} K^{-1}$ ) reported for  $Ni_3Al$  [23] and  $Co_3(Al, W)$  [24,25]. SAED patterns of Pt-27at.%Al taken along the  $[110]$  direction before and after cooling to 173 K are shown in Figs. 2(g) and (h), respectively. Additional diffraction spots appear after cooling at positions indicated by arrows in Fig. 2(h). In view of the fact that orientation domains are expected to form during the cubic ( $L1_2$ ) to tetragonal (either  $D0c$ ,  $D0c'$  or  $Pt_3Ga$  structures) phase transformation, the observed SAED pattern of Fig. 2(h) cannot be ascribed uniquely to one of the three candidate tetragonal structures without the knowledge of the domain size. One of the three domains can produce the observed SAED pattern in the case of the  $Pt_3Ga$  structures, whereas not only one of the three domains but also their superposition can do so in the case of the  $D0c$  and  $D0c'$  structures. Another inspection of SAED patterns along other directions such as  $\langle 111 \rangle$  is needed to conclude this. Nevertheless, we

---

\*Although the unit cell of all possible tetragonal structures ( $D0c$ ,  $D0c'$  and  $Pt_3Ga$  structures) is usually taken to be  $\sqrt{2}a \times \sqrt{2}a \times 2a$  when expressed with the lattice constant  $a$  of the  $L1_2$  structure, Miller indices to express crystallographic planes and directions (in Figs. 2(d)-(f) and (h)) are given with respect to the  $L1_2$  phase for the ease of understanding.

suspect the low temperature phase is either D0c or D0c' structure, on the assumption that the area from which the SAED pattern is formed is sufficiently larger than the domain size. We have confirmed that the transformation between the cubic L1<sub>2</sub> and tetragonal phases occurs reversibly through thermal cycling experiments made with the cryo-TEM stage.

All these indicate that at the alloy composition of Pt-27at.%Al, the L1<sub>2</sub> phase is stable only above ~220 K. This is consistent qualitatively with the results of experiment [20,21] and calculation [18,19].

### 3.2. Elastic constants

Values of single-crystal elastic constants determined for Pt<sub>3</sub>Al (Pt-27at.%Al) at room temperature where the L1<sub>2</sub> phase is stable are tabulated in Table 1 together with those calculated for Pt<sub>3</sub>Al [19, 26] and those experimentally determined for Ni<sub>3</sub>Al [27] and Ni<sub>3</sub>Ge [28]. The values of all the three independent single-crystal elastic constants of Pt<sub>3</sub>Al experimentally determined in the present study are generally much larger than those experimentally determined for Ni<sub>3</sub>Ge and Ni<sub>3</sub>Al. This is also the case for polycrystalline elastic constants. These may be due to the fact that the melting point of Pt<sub>3</sub>Al is higher than that of the other two compounds. The values of all the three independent elastic constants of Pt<sub>3</sub>Al experimentally determined in the present study differ considerably from those calculated for the same compound [19, 26], although those calculated by Chauke et al. [19] are closer to the experimental values. One of the reasons for this discrepancy may be the difference in the alloy composition and temperature. Chauke et al. [19] indeed calculated for hypothetical L1<sub>2</sub>-Pt<sub>3</sub>Al with the stoichiometric composition at 0 K, knowing that the ground state of stoichiometric Pt<sub>3</sub>Al is the Pt<sub>3</sub>Ga structure. A noticeable difference in the elastic constants between experiment and calculation can be found in the anisotropic parameter value. While both calculations predict very low values (1.30 and 1.47) for the anisotropic parameter, the present experiment indicates that the value (1.75) is not as low as that predicted by calculation. The anisotropic parameter value of Pt<sub>3</sub>Al is indeed comparable to that determined for Ni<sub>3</sub>Ge [28], although the value is still considerably lower than that of Ni<sub>3</sub>Al [27].

When judged from the values of Poisson's ratio (0.331), Cauchy pressure (+84 GPa; defined as  $c_{12}-c_{44}$  for crystals of the cubic symmetry) and  $G$  (shear modulus)/ $B$  (bulk modulus) ratio (0.382), significant brittleness is not expected for Pt<sub>3</sub>Al, although the previous deformation experiments [7,8] indicate the brittleness of Pt<sub>3</sub>Al even in the single-crystal form, in which instantaneous failure occurs soon after yielding (in the

plastic strain range of 0.1-0.2%).

### **3.3. Stress-strain behaviour and slip trace analysis**

Figures 4(a)-(c) show typical stress-strain curves obtained at selected temperatures for the [001],  $[\bar{1} 2 12]$  and  $[\bar{2} 34]$  orientations, respectively. All specimens can be easily deformed without failure generally at least up to the plastic strain level of 1 %, being consistent with the expected deformability of the  $L_{12}$  phase from the present result of the single-crystal elastic constants measurement. This is in significant contrast to the brittleness reported for the same  $L_{12}$  compound [7,8]. However, failure seems to occur soon after yielding at a plastic strain level of 0.2-0.3% for the [001]-oriented crystals when the deformation temperature is below 473 K. Of course, if the deformation temperature is decreased sufficiently so that the  $L_{12}$  phase is no longer the stable one, failure is observed to occur soon after yielding at a plastic strain level of 0.2-0.3%, as in the case of the  $[\bar{1} 2 12]$  orientation at 77 K. The most remarkable feature in the stress-strain curves is that generally the work hardening rate after yielding is very low. The value of the work-hardening rate is mostly low, in the range of 1-5 GPa, and does not depend much on temperature. This is in significant contrast to the case of many other  $L_{12}$  compounds based on  $Ni_3Al$ , in which the value of the work-hardening rate is very high (5-50 GPa) and depends on temperature [1]. This may indicate that the deformation mechanism of  $Pt_3Al$  is different from that of  $Ni_3Al$ -based  $L_{12}$  compounds. Another feature noted in the stress-strain curves is the occurrence of serrated flow observed for the  $[\bar{2} 34]$  orientation above 673 K, at which the yield stress tends to increase with the increase in temperature.

The values of yield stress deduced as the 0.2% off-set flow stress are plotted in Fig. 5 as a function of temperature. If we extend the plot down to the low temperature region where the  $L_{12}$  phase is no longer stable, the yield stress obviously decreases very rapidly with increasing temperature at low temperatures for both the  $[\bar{2} 34]$  and  $[\bar{1} 2 12]$  orientations with the extent of the increase in yield stress being more significant for the  $[\bar{2} 34]$  orientation in which slip is expected to occur on the (001) cube plane. This is consistent with the observation by Wee et al [7] and Heredia et al. [8]. However in the temperature range where the  $L_{12}$  phase is stable, the temperature dependence of yield stress is not so significant, although there is a general tendency that the yield stress decreases with increasing temperature. One of the exceptions to this is the slight increase in yield stress with temperature observed between room temperature and 473 K for the [001] orientation. As stated above, however, cracking is usually observed soon after yielding for the corresponding deformation conditions. The observed slight

increase in yield stress may thus be related to a scatter in yield stress occurring when yielding is accompanied by cracking. Further study is definitely needed to conclude this. Another exception is the moderate increase in yield stress observed above 673 K for the  $[\bar{2} 34]$  orientation. A similar increase in yield stress is also observed by Wee et al [7] and Heredia et al. [8]. One point to be noted is that the stress-strain curve in the corresponding condition is usually accompanied by serrated flow, as indicated in the inset in Fig. 4(c).

Slip lines observed for the  $[\bar{2} 34]$  orientation are exclusively those corresponding to (001) cube slip in the whole temperature range investigated, as seen in Fig. 6. This is consistent with the fact that the maximum Schmid factor (0.487) for (001) cube slip is larger than that (0.422) for (111) octahedral slip for this orientation. Slip lines observed for this orientation are always sharp and straight. On the other hand, slip lines observed for the [001] orientation are generally wavy in the whole temperature range investigated (Fig. 7), suggesting the frequent occurrence of cross slip. Since no shear stress is exerted on any {001} cube planes, slip lines observed are exclusively those corresponding to {111} octahedral slip. Cross-slip is thus considered to occur from one of {111} octahedral slip planes to another octahedral slip plane very easily. For the  $[\bar{1} 2 12]$  orientation, the maximum Schmid factor (0.463) for (111) octahedral slip is 2.7 times larger than that (0.171) for (001) cube slip. At high temperatures above 673 K, slip lines observed are wavy and are exclusively those corresponding to {111} octahedral slip with (111) being the major octahedral slip plane and with frequent cross-slip among octahedral planes (Fig. 8). As the deformation temperature is lowered below 473 K, slip tends to occur preferentially on (001) cube slip. Slip lines observed at 473 K are exclusively those corresponding to (001) cube slip, while at room temperature, the occurrence of (001) cube slip and the subsequent occurrence of (111) slip are noted (Fig. 8). The observed slip planes are indicated in the yield stress versus temperature curves of Fig. 5 with different symbols.

### **3.4. Dislocation structures**

#### **3.4.1. (001) slip**

Figures 9(a)-(c) shows typical dislocation structures observed in  $[\bar{2} 34]$ -oriented specimens deformed at room temperature, 673 K and 1073 K, respectively. Below 673 K, where the yield stress gradually decreases with the increase in temperature (Fig. 5), dislocations tend to roughly align along their edge orientation, many of which frequently form dipoles (Figs. 9(a) and (b)), as confirmed by imaging with two opposite reflection vectors. Their alignment along the edge orientation is only



on the overall scale and each of them is indeed smoothly curved without any preferred orientation. This suggests that the Peierls stress for the motion of screw dislocations may not be so high as expected from the results of atomistic calculation by Vitek and co-workers [4,10-14] that the core of the screw APB-coupled superpartial dislocation with  $\mathbf{b} = 1/2\langle 110 \rangle$  is always non-planar on the (001) cube plane and hence experiences a high Peierls stress for the motion. At 1073 K, where the yield stress gradually increases with the increase in temperature (Fig. 5), dislocations do not align along their edge orientation any more. Although some dislocations tend to align along a particular directions (for examples, along the screw orientation and along a direction about 60° inclined from  $[10\bar{1}]$  on (001), as indicated by S and D in Fig. 9(c)), they are different from those noted as cube-edge orientations for (001) cube slip in Fe<sub>3</sub>Ge [29,30].

The dissociation scheme of dislocations with  $\mathbf{b}$  (Burgers vector) =  $[1\bar{1}0]$  gliding on the (001) slip plane in a  $[\bar{2}34]$ -oriented specimen deformed at room temperature is analysed in Fig. 10. A two-fold dissociation is observed along the dislocations imaged in Figs. 10(a) and (b) under  $\mathbf{g}$  (reflection vectors) =  $2\bar{2}0$  and  $\bar{2}20$ , respectively. The reversal of the peak asymmetry upon reversing  $\mathbf{g}$  is consistent with a dissociation of a dislocation with  $\mathbf{b} = [1\bar{1}0]$  into two partials with collinear Burgers vectors  $\mathbf{b}_p = 1/2[1\bar{1}0]$  separated by an APB on the (001) slip plane. The dissociation mode is confirmed by the fact that both partials are simultaneously out of contrast when imaged with  $\mathbf{g} = 220$  (Fig. 10(c)) and  $\mathbf{g} = \bar{1}\bar{1}1$  (Fig. 10(d)). Essentially the same results are obtained at all temperatures. The apparent dissociation widths ( $4.8 \pm 0.4$  nm on average) between superpartial dislocations of the edge orientation at room temperature are corrected using the image shift correction method of Cockayne [31] and the shear modulus determined in the present study and they are compared with those calculated with the DISDI program [32] which incorporates the elastic anisotropy. The APB energy on (001) ( $\gamma_{APB}^{(001)}$ ) is estimated as  $361 \pm 35$  mJ/m<sup>2</sup>. The APB energy on (001) depends on temperature so that the apparent dissociation widths between superpartial dislocations of the edge orientation change from 4.8 nm at room temperature to  $5.0 \pm 0.4$  nm at 673 K and to  $5.7 \pm 0.4$  nm at 1073 K (on the basis of TEM measurements made at room temperature). The APB energies on (001) are similarly calculated to be  $352 \pm 30$  mJ/m<sup>2</sup> at 673 K and  $305 \pm 25$  mJ/m<sup>2</sup> at 1073 K.

### 3.4.2. (111) slip

Figures 11(a)-(c) shows typical dislocation structures observed in  $[\bar{1}2]$ -oriented specimens deformed at room temperature, 673 K and 1073 K, respectively. Below 673 K, dislocations have a strong tendency to align along their screw orientation,

forming many cusps and prismatic loops (Figs. 11(a) and (b)). This indicates that screw dislocations experience a high Peierls stress for their motion and that cross-slip occurs very frequently (consistently with the slip trace observations of Fig. 8), as in many body-centred cubic (bcc) metals. At 1073 K, only short segments of dislocations are observed to lie on the (111) slip plane, indicating the deformation temperature is high enough for the climb motion to occur significantly. The alignment of dislocations along their screw orientation is consistent with the postulation by Vitek and co-workers [4,10,11,14] based on the results of atomistic calculation that the core of each of the SISF-coupled superpartial dislocations with  $\mathbf{b} = 1/3\langle 112 \rangle$  is non-planar along the screw orientation. However, the actual dissociation scheme of dislocations with  $\mathbf{b} = [10\bar{1}]$  gliding on the (111) slip plane is not consistent with what is expected by Vitek and co-workers [4,10,11,14], as shown below.

The dissociation scheme of dislocations with  $\mathbf{b} = [10\bar{1}]$  gliding on the (111) slip plane in a  $[\bar{1} \ 2 \ 12]$ -oriented specimen deformed at room temperature is analysed in Fig. 12. A two-fold dissociation is also observed along the dislocations imaged in Figs. 12(a) and (b) under  $\mathbf{g} = 20\bar{2}$  and  $\bar{2} \ 02$ , respectively. The reversal of the peak asymmetry upon reversing  $\mathbf{g}$  is consistent with a dissociation of a dislocation with  $\mathbf{b} = [10\bar{1}]$  into two partials with collinear Burgers vectors  $\mathbf{b}_p = 1/2[10\bar{1}]$  separated by an APB on the (111) slip plane. This is indeed confirmed by the fact that both partials are simultaneously out of contrast when imaged with  $\mathbf{g} = 1\bar{1}1$  (Fig. 12(c)) and  $\mathbf{g} = 020$  (Fig. 12(d)). As is clear from the comparison with Fig. 12(e), which is imaged with  $\mathbf{g} = 20\bar{2}$  along near  $[010]$  (the normal to the possible cube cross-slip plane), the APB width is the largest when imaged along  $[111]$  (the normal to the (111) slip plane), which is in contrast to the case of most  $\text{Ni}_3\text{Al}$ -based  $\text{L}_{12}$  compounds where the APB width for  $\langle 110 \rangle$  dislocations locked in the Kear-Wilks configuration along the screw orientation is larger on the cube cross-slip plane than on the octahedral slip plane. This indicates that cross slip usually occurs between octahedral slip planes but not from octahedral to cube slip planes and vice versa. The APB energy on (111) ( $\gamma_{APB}^{(111)}$ ) is similarly calculated from the apparent dissociation widths ( $3.0 \pm 0.3$  nm on average) between superpartial dislocations of the screw orientation to be  $496 \pm 104$  mJ/m<sup>2</sup> at room temperature. The APB energy on (111) may also depend on temperature as in the case of the APB energy on (001) but has yet been addressed.

## 4. Discussion

### 4.1. Temperature dependence of CRSS for slip on (001) and (111)

Using the corresponding Schmid factors, the critical resolved shear stress

(CRSS) for slip on (001) and (111) was calculated as a function of temperature and the results obtained are shown in Fig. 13. The values of CRSS for slip on (111) are always higher than those for slip on (001) in the whole temperature range investigated. This is consistent with the results obtained by Wee et al. [7] and Heredia et al. [8]. The CRSS for slip on (111) does not depend much on crystal orientation in the whole temperature range investigated. This seems also the case for slip on (001), although the data point is limited only to that at room temperature. Although the ratio of Schmid factors for slip on (001) to that for slip on (111) is quite different for the two orientations investigated (0.635 and 1.16, respectively, for  $[\bar{1}26]$  and  $[\bar{2}34]$  orientations), the values of CRSS coincide with each other within 6 % at room temperature. The Schmid law, thus, holds true for slip both on (001) and on (111). Although Wee et al. [7] and Heredia et al. [8], who used single crystals with a composition exactly the same as that used in the present study, reported that the CRSS for both slip rapidly decreases with the increase in temperature at low temperatures, this conclusion cannot be drawn from the CRSS versus temperature curves of Fig. 13 because the  $L_{12}$  phase is no longer the stable phase below  $\sim 220$  K. The possibility of showing the normal (large negative) temperature dependence of CRSS at low temperatures as well as the reason for the absence of the anomalous (positive) temperature dependence of CRSS for slip on (111) at high temperatures will be discussed separately in the following.

#### ***4.2. Normal (negative) temperature dependence of CRSS at low temperatures***

As described above, the large negative temperature dependence of CRSS observed for slip both on (001) and (111) in  $Pt_3Al$  by Wee et al. [7] and Heredia et al. [8] does not represent the real deformation behaviour of the  $L_{12}$  structure, in view of the fact that the  $L_{12}$  phase is no longer the stable phase below  $\sim 220$  K at the chemical composition of Pt-27at.%Al. The CRSS for slip in either  $D0c$  or  $D0c'$  structures is expected to be higher than that for the corresponding slip in  $L_{12}$  structure, owing to the possible formation of domain structures (due to the cubic to tetragonal phase transformation) and the more complex crystal structure accompanied by displacement of some of Pt atoms from the corresponding atom sites in the  $L_{12}$  structure. This is consistent with the prediction from first-principles calculations by Gornostyrev et al. [18] and also with the experimental results by Oya-Seimiya et al. [9] who pointed out that the increase in yield stress at low temperature is more steep as the alloy composition becomes closer to the stoichiometric composition. For the  $L_{12}$  phase of  $Pt_3Al$  to be stable down to a very low temperature, the alloy composition should be considerably rich in Al, since the phase transformation temperature decreases with the

increase in the Al concentration in the Al-rich compositions [20,21]. Our preliminary experiment indeed indicates the absence of the phase transformation at least down to 77 K at the composition of Pt-29at.%Al. A study is under way in our group to elucidate the real deformation behaviour of the  $L1_2$  structure of  $Pt_3Al$  at low temperatures with single crystals of Pt-29at.%Al.

Nevertheless, we believe that if the  $L1_2$  phase of  $Pt_3Al$  is assumed to be stable down to a low temperature, the CRSS for slip on (111) should decrease rapidly with the increase in temperature when judged from the high Peierls stress for the motion of dislocations with  $\mathbf{b} = \langle 110 \rangle$  expected from the predominant alignment along their screw orientation at room temperature (Fig. 11(a)), resembling that observed in many bcc metals. Of importance to note here is that the large negative temperature dependence of CRSS for slip on (111) is expected to be carried by the motion of APB-coupled superpartials with  $\mathbf{b} = 1/2\langle 110 \rangle$ , but not by the motion of SISF-coupled superpartials with  $\mathbf{b} = 1/3\langle 112 \rangle$ , as often and usually assumed [4,10-12,14]. This is consistent with the predictions from first-principles calculations by Paxton et al. [17] and Gornostyrev et al. [18] who pointed out that the SISF energy is comparably as high as the APB energy on (111) in  $Pt_3Al$ . Vitek and Paidar [4] recently showed that when the CSF (complex stacking fault) is either unstable or its energy is so high that splitting into Shockley partials cannot take place, the core of superpartials with  $\mathbf{b} = 1/2\langle 110 \rangle$  bounding an APB on (111) can be non-planar, spreading into two different octahedral  $\{111\}$  planes at least along the screw orientation, in contrast to the planar core configuration usually assumed for the same superpartials with  $\mathbf{b} = 1/2\langle 110 \rangle$  in  $Ni_3Al$ . We believe that dislocations, which are observed in the present study to dissociate into two collinear superpartials  $\mathbf{b} = 1/2\langle 110 \rangle$  bounding an APB on (111), have the non-planar core structure as calculated by Vitek and Paidar [4]. This may indicate that the CSF energy is very high in  $Pt_3Al$ . This is generally consistent with the results of first principle calculations [17,18,33], as tabulated in Table 2.

We also believe that the CRSS for slip on (001) decreases rapidly with the increase in temperature at low temperatures (if the  $L1_2$  phase is assumed to be stable down to a low temperature), since the core of superpartials with  $\mathbf{b} = 1/2\langle 110 \rangle$  bounding an APB on (001) is generally believed to be non-planar at least along the screw orientation [4,10-12,14]. However, the decrease in the CRSS for slip on (001) may not occur so rapidly when judged from the present observation that the deformation structure at room temperature is dominated by smoothly curved edge dislocations rather than screw dislocations that are believed to experience a high Peierls stress due to the non-planar core structure. This is consistent with the fact that the CRSS for slip on

(001) is always lower than that for slip on (111) (Fig. 13). The absence of any strong orientation dependence of CRSS for slip on (001) may be interpreted in the same line.

In Fe<sub>3</sub>Ge in which slip is known to occur on the (001) cube plane, dislocations are observed to dissociate into two collinear superpartials with  $\mathbf{b} = 1/2\langle 110 \rangle$  separated by an APB on {001} without any preferred orientation after deformation at room temperature [29,30]. This is consistent with what is observed for slip on (001) in Pt<sub>3</sub>Al. The reason why slip on (111) is not observed to operate in polycrystals of Fe<sub>3</sub>Ge is postulated to be caused by the considerably higher CRSS for slip on (111) than for slip on (001). We believe that even in Fe<sub>3</sub>Ge, slip on (111) should be observed when a single crystal is deformed along the [001] orientation, as in Pt<sub>3</sub>Al. If the considerably higher CRSS for slip on (111) than for slip on (001) is due to the non-planar core structure of the superpartial dislocation with  $\mathbf{b}=1/2\langle 110 \rangle$  bounding an APB on (111), the CSF energy may also be very high in Fe<sub>3</sub>Ge and we may conclude that the high CSF energy tends to make L1<sub>2</sub> compounds to slip preferentially on the (001) cube plane rather than on the (111) octahedral plane.

#### ***4.3. Absence of the anomalous (positive) temperature dependence of CRSS at high temperatures***

The absence of the anomalous (positive) temperature dependence of CRSS at high temperatures for slip on (111) in Pt<sub>3</sub>Al has been interpreted in terms of the occurrence of the SISF-type dissociation for the  $[\bar{1}01]$  dislocation gliding on the (111) plane, which makes the cross-slip from (111) to (010) irrelevant. In the present study, however, the dissociation scheme for the  $[\bar{1}01]$  dislocation gliding on the (111) plane is indeed proved to be of the APB-type, as usually observed in many L1<sub>2</sub> compounds based on Ni<sub>3</sub>Al [1-4,25]. Then, a renewed question arises as to why the anomalous (positive) temperature dependence of CRSS is absent for slip on (111) for Pt<sub>3</sub>Al, even though the dissociation scheme is of the APB-type.

The anomalous temperature dependence of CRSS for slip on (111) in many L1<sub>2</sub> compounds is generally believed to be due to the thermally activated cross-slip of dislocations with  $\mathbf{b} = [\bar{1}01]$  dissociated in the scheme of the APB-type from (111) octahedral to (010) cube planes. Paidar et al. [13] pointed out that APB-coupled superpartial is driven to cross-slip onto (010) from (111) if the APB energy on (001) is smaller than that on (111), so that the condition is described as  $\lambda (= \gamma_{APB}^{(001)} / \gamma_{APB}^{(111)}) < 3^{-1/2}$ . Yoo [16] subsequently demonstrated that a torque force acting between screw APB-coupled superpartial pair assist the cross slip so as to rotate them towards the cube plane in the anisotropic medium. Then, the condition for cross-slip is described as  $\lambda < B$ ,

where B is a dimensionless parameter of elastic constants,  $B = 3^{1/2}A/(A+2)$  expressed with the Zener anisotropy ratio,  $A = 2c_{44}/(c_{11}-c_{12})$ . Saada and Veyssi re [34] further pointed out that, even if the driving force for the cross slip is initially negative, the dissociation on the (010) plane is favoured energetically over that on the (111) plane so that the condition for cross-slip to occur is relaxed to  $\lambda < 3^{1/4}B^{1/2}$ . Based on the above argument on the condition for cross-slip, Paxton and Sun [33] proposed the  $\lambda$ -B map to predict the energetics for the stability of the APB-coupled  $[\bar{1}01]$  dislocation on (111) and (001) planes and, thus, to show the necessary condition for the yield stress anomaly to occur. The  $\lambda$ -B map can be constructed by plotting the values of  $\lambda$  and B for the corresponding L1<sub>2</sub> compounds, as shown in Fig. 14 for some typical L1<sub>2</sub> compounds. The yield stress anomaly is predicted to occur for those L1<sub>2</sub> compounds plotted in the regions C and C', since dissociation on the (010) cube plane has a lower energy than that on the (111) octahedral plane in these domains. Indeed, those L1<sub>2</sub> compounds that are known to exhibit the yield stress anomaly such as Ni<sub>3</sub>Al, Co<sub>3</sub>Ti, Ni<sub>3</sub>Si and Ni<sub>3</sub>Ge are plotted in the regions C and C' [33,35]. In the regions O' and O, on the other hand, dissociation on the (111) plane is more favourable energetically than on the (010) plane and the yield stress anomaly is not predicted to occur. Paxton et al., who pointed out that the dissociation scheme of the APB-type is preferred to that of the SISF-type in Pt<sub>3</sub>Al, based on their theoretical calculation of energies of APB and SISF on (111) [17], plotted Pt<sub>3</sub>Al in the region O' in the  $\lambda$ -B map with the calculated values of the APB energies on (111) and (010) [33] and elastic constants [26]. The absence of the yield stress anomaly for slip on (111) in Pt<sub>3</sub>Al was, thus, interpreted in terms of the high value of  $\lambda$  ( $\lambda=1.50$ ;  $\gamma_{APB}^{(001)} > \gamma_{APB}^{(111)}$ ) and the low value of B (with A=1.47). In the present study, however, the value of  $\lambda$  and B are determined experimentally for Pt<sub>3</sub>Al with an off-stoichiometric composition (Pt-27at.%Al) to be significantly different from those theoretically calculated [17,18]. The value of  $\lambda$  is 0.728 ( $\gamma_{APB}^{(001)} < \gamma_{APB}^{(111)}$ ) and the value of B is 0.807 (with A=1.75), both of which are favourable to promote the transformation of the screw dislocation from (111) dissociation to (010) dissociation. With these experimental values, Pt<sub>3</sub>Al is indeed plotted in the region of C, as are many other L1<sub>2</sub> compounds known to exhibit the yield stress anomaly. Of interest to note in the  $\lambda$ -B map of Fig. 14 is that Fe<sub>3</sub>Ge that is known to slip preferentially on the cube (001) plane is also plotted in the region C, although it is not yet known whether it exhibits an anomaly in CRSS when slip is forced to occur on the (111) plane (for the [001] orientation) or not. The reason for this discrepancy (the location of Pt<sub>3</sub>Al and possibly

Fe<sub>3</sub>Ge in the region C) is unclear as yet, although Fe<sub>3</sub>Ge is claimed as a L1<sub>2</sub> compound in which the dissociation of <110> dislocation is expected to occur according to the scheme of the SISF-type on (111) from first-principle calculations [35]. In view of the expected high values of the CSF energy for these two compounds, the effects of the CSF energy may be properly taken into account in the prediction for the occurrence of the yield stress anomaly in L1<sub>2</sub> compounds using a similar map. The importance of the CSF energy and the corresponding dissociation has indeed been recognised in determining the rate of cross-slip in L1<sub>2</sub> compounds based on Ni<sub>3</sub>Al [36-38].

## 5. Conclusions

(1) For Pt<sub>3</sub>Al with an off-stoichiometric composition of Pt-27at.%Al, the L1<sub>2</sub> structure is no longer stable below around 220 K. It is either D0c or D0c' structure that is stable below 220K. Owing to this phase transformation, no detailed description can be made for the deformation behaviour of L1<sub>2</sub>-Pt<sub>3</sub>Al at low temperature, although Pt<sub>3</sub>Al is frequently referred to as a representative L1<sub>2</sub> compound that exhibits a very large negative temperature dependence of yield stress, which is often called the 'normal' temperature dependence of yield stress.

(2) Slip in Pt<sub>3</sub>Al occurs along <110> both on (001) cube and on (111) octahedral planes with slip on (001) being the primary slip system that operates in most crystal orientations except for a narrow orientation region close to [001] in the stereographic projection. The values of CRSS for slip on (001) are always lower than those for slip on (111) in the whole temperature range investigated, and the Schmid law holds true for slip both on (001) and on (111).

(3) When slip occurs on (001), slip lines are sharp and straight, and dislocations with  $\mathbf{b} = [\bar{1}01]$  dissociate into two collinear superpartials with  $\mathbf{b} = 1/2[\bar{1}01]$  separated by an APB on (001). The CRSS decreases gradually with the increase in temperature up to 673K, above which it increases slightly with temperature, ~~which is ascribed to a dislocation-impurity interaction such as in the Portevin-Le Chatelier effect.~~

(4) When slip occurs on (111), slip lines are generally wavy in the whole temperature range investigated, suggesting the frequent occurrence of cross-slip from one of {111} octahedral slip planes to another octahedral slip plane. Dislocations with  $\mathbf{b} = [\bar{1}01]$  dissociate into two collinear superpartials with  $\mathbf{b} = 1/2[\bar{1}01]$  separated by an APB on (111), and they tend to align along their screw orientation at room temperature, forming cusps and prismatic loops. The preferential alignment of these dislocations along the screw orientation evidently suggests the high Peierls stress for their motion and, thus, if

the  $L1_2$  phase of  $Pt_3Al$  is stable down to low temperatures, a large negative temperature dependence of CRSS is expected to be carried by the motion of APB-coupled superpartials with  $\mathbf{b} = 1/2\langle 110 \rangle$ , but not by the motion of SISF-coupled superpartials with  $\mathbf{b} = 1/3\langle 112 \rangle$ .

(5) The values of the APB energies on (111) and (010) and the single crystal elastic constants determined experimentally for  $Pt_3Al$  with an off-stoichiometric composition (Pt-27at.%Al) are found to be significantly different from those theoretically calculated for the stoichiometric compound. The low value of  $\lambda (\gamma_{APB}^{(001)} / \gamma_{APB}^{(111)})$  and the rather high value of  $B$  resulting from the rather high value of elastic anisotropy parameter ( $A$ ), both of which are favourable to promote the transformation of the APB-coupled screw dislocation from (111) dissociation to (010) dissociation, indicate that  $Pt_3Al$  is predicted in the  $\lambda$ - $B$  map to exhibit the yield stress anomaly for slip on (111), which is not consistent with the result of experiment.

#### Acknowledgements

This work was supported by Grant-in-Aid for Scientific Research (A) (No.21246101 and No.21360337) from the Ministry of Education, Culture, Sports, Science and Technology (MEXT) Japan and in part by the Global COE (Center of Excellence) Program of International Center for Integrated Research and Advanced Education in Materials Science from the MEXT Japan. The authors are grateful to Dr. K. Tanaka of Kobe University for allowing us to use the apparatus for the measurement of the elastic constants.



## References

- [1] P. Veyssi re and G. Saada, *Microscopy and plasticity of the  $L1_2$   $\gamma$  phase*, in *Dislocations in Solids*, Vol. 10, F. R. N. Nabarro and M. S. Duesbery, eds., Elsevier, Amsterdam, 1996, p. 253.
- [2] D.P. Pope and S.S. Ezz, *Int. Metals Rev.* 29 (1984) p.136.
- [3] C.T. Liu and D.P. Pope, *Ni<sub>3</sub>Al and its Alloys*, in *Intermetallic Compounds Principles and Practice* Vol. 2, J. H. Westbrook and R. L. Fleischer, eds., John Wiley & Sons, Chichester, England, 1995, p. 17.
- [4] V. Vitek and V. Paidar, *Non-Planar Dislocation Cores: A Ubiquitous Phenomenon Affecting Mechanical Properties of Crystalline Materials*, in *Dislocations in Solids*, Vol. 14, J.P. Hirth, eds., Elsevier, Amsterdam, 2008, p. 441.
- [5] D.M. Wee and T. Suzuki, *Trans. Japan Inst. Metals* 20 (1979) p. 634.
- [6] D.M. Wee, O. Noguchi, Y. Oya and T. Suzuki, *Trans. Japan Inst. Metals* 21 (1980) p. 237.
- [7] D.M. Wee, D.P. Pope and V. Vitek, *Acta Metall.* 32 (1984) p. 829.
- [8] F.E. Heredia, G. Tichy, D.P. Pope and V. Vitek, *Acta Metall.* 37 (1989) p.2755.
- [9] Y. Oya-Semiya, T. Shinoda and T. Suzuki, *Mater. Trans.* 37 (1996) p.1464.
- [10] V. Paidar, D.P. Pope and M. Yamaguchi, *Scripta Metall.* 15 (1981) p.1029.
- [11] M. Yamaguchi, V. Paidar, D.P. Pope and V. Vitek, *Phil. Mag. A* 45 (1982) p.867.
- [12] V. Paidar, M. Yamaguchi, D.P. Pope and V. Vitek, *Phil. Mag. A* 45 (1982) p.883.
- [13] V. Paidar, D.P. Pope and V. Vitek, *Acta Metall.* 32 (1984) p.435.
- [14] G. Tichy, V. Vitek and D.P. Pope, *Phil. Mag. A* 53 (1986) p.467.
- [15] P.A. Flinn, *Trans. Metal. Soc. AIME* 218 (1960) p.145.
- [16] M.H. Yoo, *Scripta Metall.* 20 (1986) p.915.
- [17] A.T. Paxton, Point, Line and Planar Defects, in *Electron Theory in Alloy Design*, D.G. Pettifor and A.H. Cottrell, eds., Institute of Materials, London, 1992, p.158.
- [18] Y.N. Gornostyrev, Y. Kontsevoi, A.J. Freeman, M.I. Katsnelson, A.V. Trefilov and A.I. Lichtenshtein, *Phys. Rev. B* 70 (2004) p.014102.
- [19] H.R. Chauke, B. Minisini, R. Drautz, D. Nguyen-Manh, P.E. Ngoepe and D.G. Pettifor, *Intermetallics* 18 (2010) p.417.
- [20] P. Guex and P. Feschotte, *J. Less-Common Met.* 46 (1976) p.101.
- [21] Y. Oya, Y. Mishima and T. Suzuki, *Z. Metallk.* 78 (1987) p.485.
- [22] K. Tanaka and M. Koiwa, *Intermetallics* 4 (1996) p.S29.
- [23] P.V. Mohan Rao, S.V. Suryanarayana, K. Satyanarayana Murthy and S.V. Nagender Naidu, *J. Phys.: Condens. Matter* 1 (1989) p.5357.

- [24] K. Tanaka, T. Ohashi, K. Kishida and H. Inui, *Appl. Phys. Lett.*, 91 (2007) p.181907.
- [25] N.L. Okamoto, T. Oohashi, H. Adachi, K. Kishida, H. Inui and P. Veyssi re, *Phil. Mag.* 91 (2011) p.3667.
- [26] C.L. Fu and M.H. Yoo, *Mater. Res. Soc. Symp. Proc.* 133 (1989) p.81.
- [27] R.W. Dickson, J.B. Wachtman and S.M. Copley, *J. Appl. Phys.* 40 (1969) p.2276.
- [28] H. Yasuda, T. Takasugi and M. Koiwa, *Acta Metall.* 40 (1992) p.381.
- [29] A.H.W. Ngan, I.P. Jones and R.E. Smallman, *Mater. Sci. Eng. A* 153 (1992) p.387.
- [30] T.J. Balk, M. Kumar and K.J. Hemker, *Acta Mater.* 49 (2001) p.1725.
- [31] D.J. Cockayne, I.L.F. Ray and M.J. Whelan, *Phil. Mag.* 20 (1969) p.1265.
- [32] J. Douin, <http://pc-web.cemes.fr/Personnel/douin/Disdi-Page.html>
- [33] A.T. Paxton and Y.Q. Sun, *Phil. Mag. A* 78 (1998) p.85.
- [34] G. Saada and P. Veyssi re, *Phil. Mag. A* 66 (1992) p.1081.
- [35] J.B. Liu, D.D. Johnson and A.V. Smirnov, *Acta Mater.* 53 (2005) p.3601.
- [36] K.J. Hemker and M.J. Mills, *Phil. Mag. A* 68 (1993) p.305.
- [37] N. Baluc and R. Schaublin, *Phil. Mag. A* 74 (1996) p.113.
- [38] H.P. Karnthaler, E.T. Muhlbacher and C. Rentenberger, *Acta Mater.* 44 (1996) p.547.

Table 1. Elastic constants of Pt<sub>3</sub>Al, Ni<sub>3</sub>Ge and Ni<sub>3</sub>Al.

	$c_{11}$ (GPa)	$c_{12}$ (GPa)	$c_{44}$ (GPa)	$c_{12} - c_{44}$ (GPa)	Anisotropic parameter, $A$	Poisson's ratio, $\nu$	$B$ (GPa)	$G$ (GPa)	$E$ (GPa)	$G/B$
Pt-27at.%Al (300 K)	336	201	117	84	1.75	0.331	246	94	250	0.382
Pt <sub>3</sub> Al <sup>[19]</sup> (0 K)	374	201	127	74	1.47	0.315	259	109	286	0.421
Pt <sub>3</sub> Al <sup>[26]</sup> (0 K)	436	220	140	80	1.30	0.311	292	126	331	0.432
Ni <sub>3</sub> Ge <sup>[27]</sup> (300 K)	221	146	124	22	3.31	0.300	171	77	200	0.450
Ni <sub>3</sub> Al <sup>[28]</sup> (300 K)	263	143	103	40	1.72	0.303	183	83	216	0.454

Table 2. Energies (in the unit of mJ/m<sup>2</sup>) of various planar faults in Pt<sub>3</sub>Al.

	$\gamma_{APB}^{(111)}$ (mJ/m <sup>2</sup> )	$\gamma_{APB}^{(001)}$ (mJ/m <sup>2</sup> )	$\gamma_{SISF}^{(111)}$ (mJ/m <sup>2</sup> )	$\gamma_{CSF}^{(111)}$ (mJ/m <sup>2</sup> )	$\lambda \left( \frac{\gamma_{APB}^{(100)}}{\gamma_{APB}^{(111)}} \right)$
Paxton et al. <sup>[33]</sup>	349	523	-	587	1.50
Paxton <sup>[17]</sup>	500	-	560	600	-
Gornostyrev et al. <sup>[18]</sup>	480	460	490	560	0.958
Present Study	496 ± 104	361 ± 35			0.728

## Figure legend

Fig. 1. Stereographic projection of compression axis orientations investigated.

Fig. 2. SAED patterns of Pt<sub>3</sub>Al with chemical compositions of (a)-(c) Pt-27at.%Al and (d)-(f) Pt-25at.%Al taken along (a),(d) [001], (b),(e) [110] and (c),(f) [111] directions at room temperature. (g) and (h) are SAED patterns of Pt-27at.%Al with the [110] incidence before and after cooling to 173 K, respectively.

Fig. 3. Thermal expansion of Pt<sub>3</sub>Al with the chemical composition of Pt-27at.%Al plotted as relative elongation with respect to the original specimen length at 89 K.

Fig. 4. Stress-strain curves of Pt<sub>3</sub>Al single crystals with (a) [001], (b)  $[\bar{1} \ 2 \ 12]$  and (c)  $[\bar{2} \ 34]$  orientations at selected temperatures. The symbol  $\times$  indicate the stress at which failure (cracking) occurs.

Fig. 5. Temperature dependence of yield stress for Pt<sub>3</sub>Al single crystals with four different orientations. Open and closed symbols indicate the occurrence of (001) cube slip and (111) octahedral slip, respectively.

Fig. 6. Slip lines observed on two orthogonal faces of  $[\bar{2} \ 34]$ -oriented crystals deformed at (a),(b) room temperature, (c),(d) 473 K, (e),(f) 673 K, (g),(h) 873 K and (i),(j) 1073 K. The compression axis is in the vertical direction.

Fig. 7. Slip lines observed on two orthogonal faces of [001]-oriented crystals deformed at (a),(b) room temperature, (c),(d) 473 K, (e),(f) 673 K, (g),(h) 873 K and (i),(j) 1073 K. The compression axis is in the vertical direction.

Fig. 8. Slip lines observed on two orthogonal faces of  $[\bar{1} \ 2 \ 12]$ -oriented crystals deformed at (a),(b) room temperature, (c),(d) 473 K, (e),(f) 673 K, (g),(h) 873 K and (i),(j) 1073 K. The compression axis is in the vertical direction.

Fig. 9. Typical dislocation structures observed in  $[\bar{2} \ 34]$ -oriented specimens deformed at (a) room temperature, (b) 673 K and (c) 1073 K, respectively. The thin foils were cut parallel to the (001) slip plane.

Fig. 10. Weak-beam images of dislocations observed in a  $[\bar{2} \ 34]$ -oriented specimen deformed at room temperature. The reflection vectors used for imaging are indicated in each of the images.

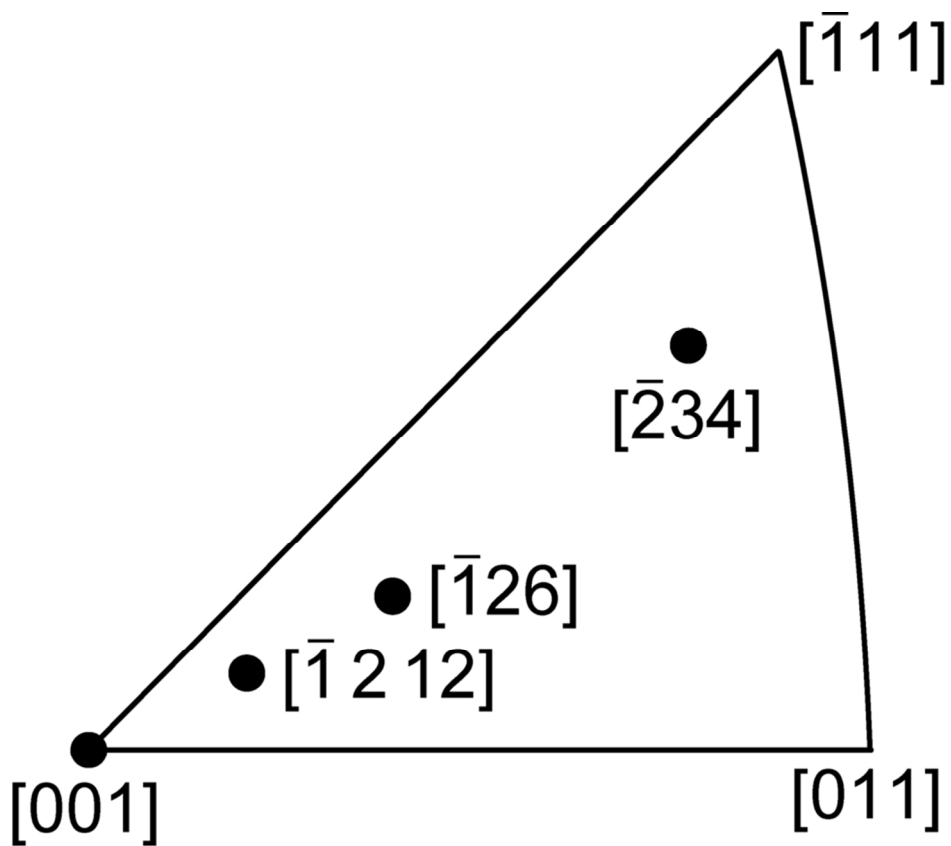
Fig. 11. Typical dislocation structures observed in  $[\bar{1} \ 2 \ 12]$ -oriented specimens deformed at (a) room temperature, (b) 673 K and (c) 1073 K, respectively. The thin foils were cut parallel to the (111) slip plane.

Fig. 12. Weak-beam images of dislocations observed in a  $[\bar{1} \ 2 \ 12]$ -oriented specimen deformed at room temperature. The reflection vectors used for imaging are indicated in each of the images. The images were taken along near (a) [111], (b)  $[\bar{1} \ 111]$ , (c) [121], and (d) [101] and (e) [010] zone-axis orientations, respectively.

Fig. 13. Temperature dependence of CRSS for slip on (001) and (111). Data points obtained from [001]-,  $[\bar{1} 2 12]$ -,  $[\bar{1} 2 6]$ - and  $[\bar{2} 3 4]$ -oriented crystals are indicated with symbols ■, ●, ▽ and △, respectively.

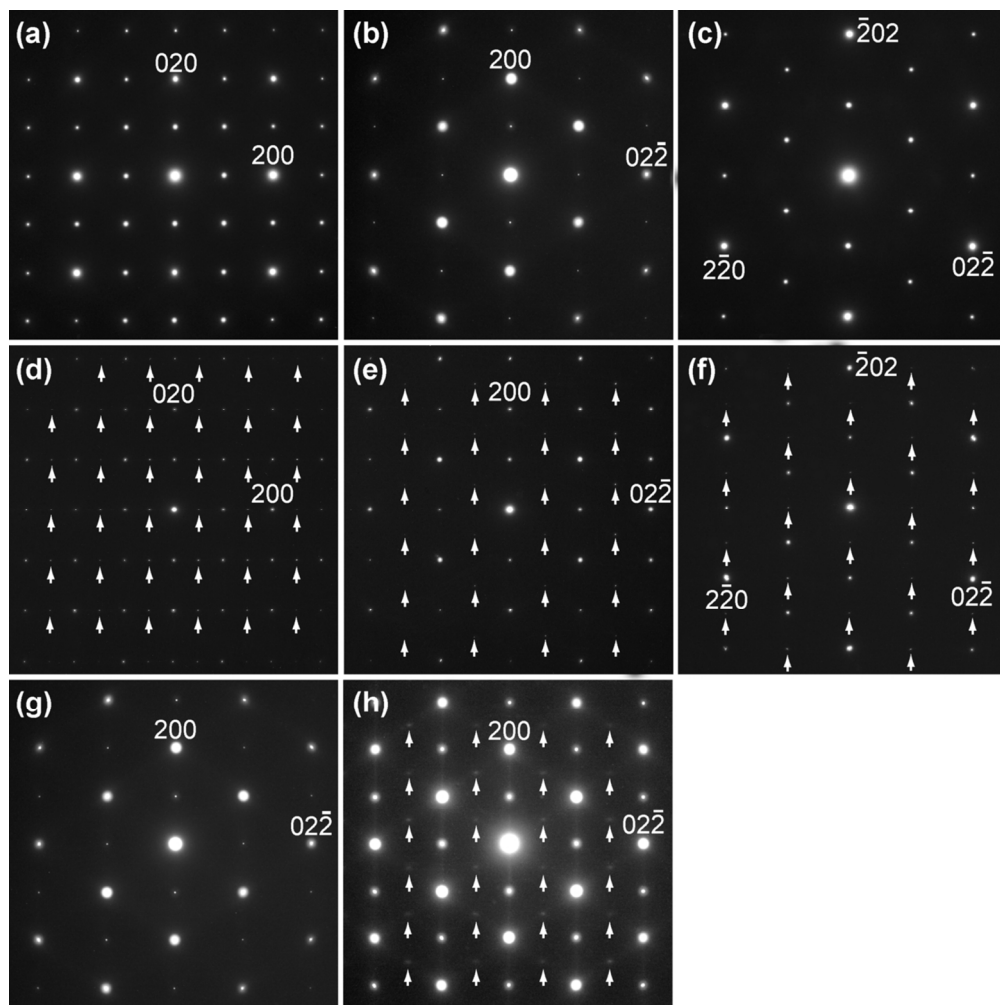
Fig. 14. The  $\lambda$ -B map proposed by Paxton et al. [33] to show the necessary condition for the yield stress anomaly to occur. The data points plotted with open symbols for Ni<sub>3</sub>Al, Co<sub>3</sub>Ti, Ni<sub>3</sub>Si, Cu<sub>3</sub>Au, Pt<sub>3</sub>Al, Ni<sub>3</sub>Ge and Fe<sub>3</sub>Ge are taken from the literature [33,35] while that plotted with the closed symbol for Pt<sub>3</sub>Al is from the present experimental result.

1  
2  
3  
4  
5  
6  
7  
8  
9  
10  
11  
12  
13  
14  
15  
16  
17  
18  
19  
20  
21  
22  
23  
24  
25  
26  
27  
28  
29  
30  
31  
32  
33  
34  
35  
36  
37  
38  
39  
40  
41  
42  
43  
44  
45  
46  
47  
48  
49  
50  
51  
52  
53  
54  
55  
56  
57  
58  
59  
60



43x37mm (600 x 600 DPI)

www Only

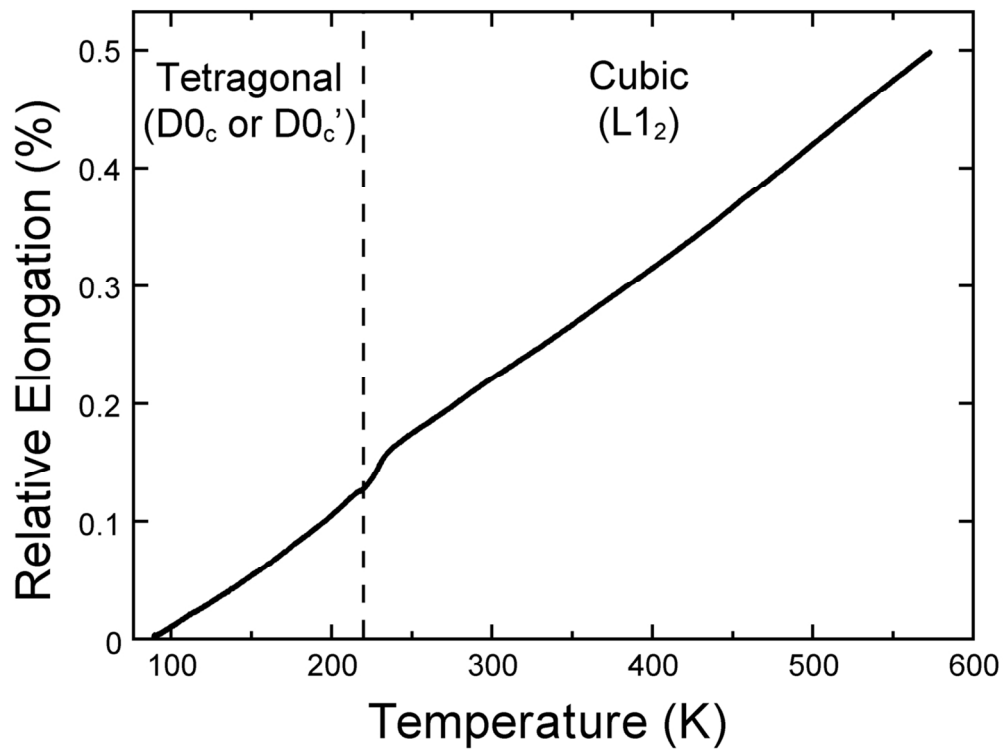


108x108mm (300 x 300 DPI)

only

1  
2  
3  
4  
5  
6  
7  
8  
9  
10  
11  
12  
13  
14  
15  
16  
17  
18  
19  
20  
21  
22  
23  
24  
25  
26  
27  
28  
29  
30  
31  
32  
33  
34  
35  
36  
37  
38  
39  
40  
41  
42  
43  
44  
45  
46  
47  
48  
49  
50  
51  
52  
53  
54  
55  
56  
57  
58  
59  
60

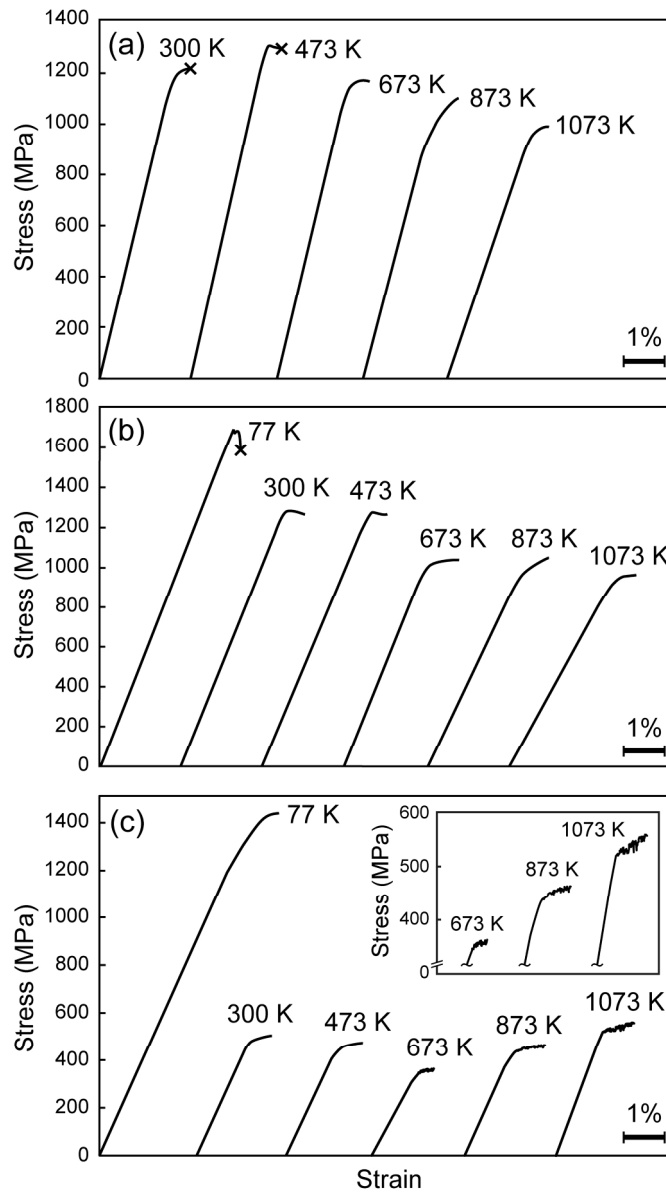




61x46mm (600 x 600 DPI)

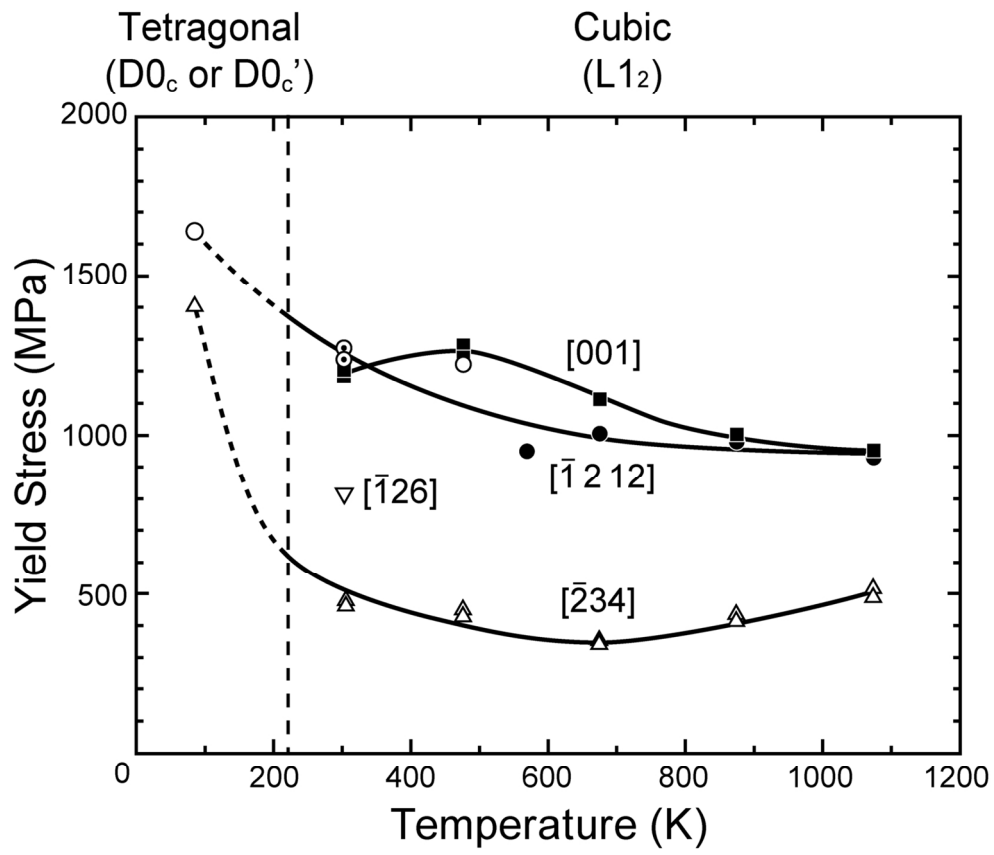
View Only

1  
2  
3  
4  
5  
6  
7  
8  
9  
10  
11  
12  
13  
14  
15  
16  
17  
18  
19  
20  
21  
22  
23  
24  
25  
26  
27  
28  
29  
30  
31  
32  
33  
34  
35  
36  
37  
38  
39  
40  
41  
42  
43  
44  
45  
46  
47  
48  
49  
50  
51  
52  
53  
54  
55  
56  
57  
58  
59  
60



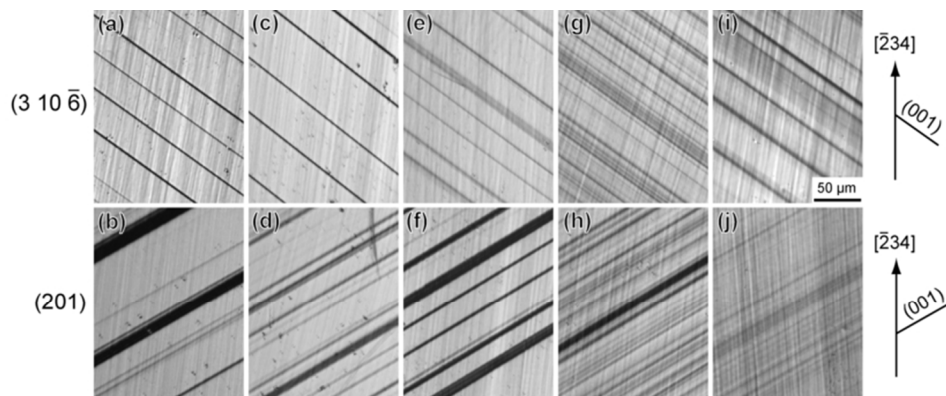
166x296mm (300 x 300 DPI)

1  
2  
3  
4  
5  
6  
7  
8  
9  
10  
11  
12  
13  
14  
15  
16  
17  
18  
19  
20  
21  
22  
23  
24  
25  
26  
27  
28  
29  
30  
31  
32  
33  
34  
35  
36  
37  
38  
39  
40  
41  
42  
43  
44  
45  
46  
47  
48  
49  
50  
51  
52  
53  
54  
55  
56  
57  
58  
59  
60



71x61mm (600 x 600 DPI)

View Only

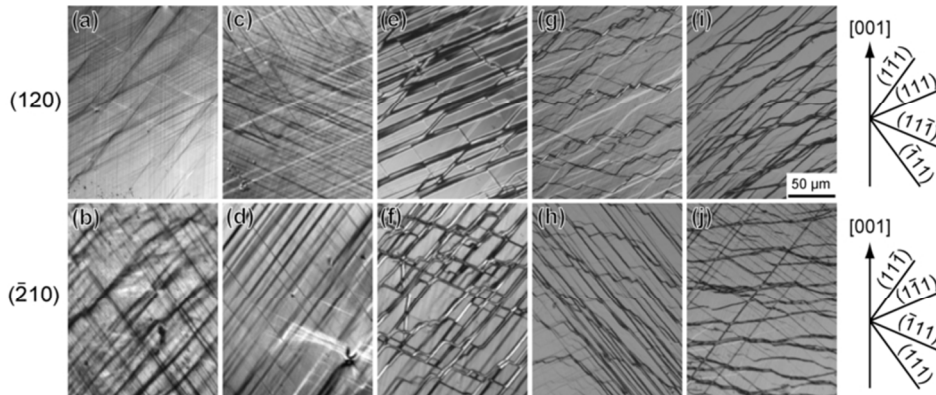


73x28mm (300 x 300 DPI)

Peer Review Only

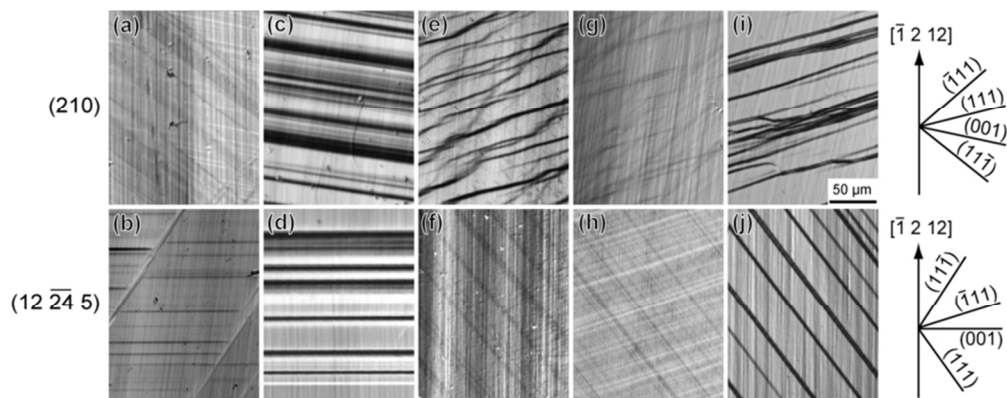
1  
2  
3  
4  
5  
6  
7  
8  
9  
10  
11  
12  
13  
14  
15  
16  
17  
18  
19  
20  
21  
22  
23  
24  
25  
26  
27  
28  
29  
30  
31  
32  
33  
34  
35  
36  
37  
38  
39  
40  
41  
42  
43  
44  
45  
46  
47  
48  
49  
50  
51  
52  
53  
54  
55  
56  
57  
58  
59  
60

1  
2  
3  
4  
5  
6  
7  
8  
9  
10  
11  
12  
13  
14  
15  
16  
17  
18  
19  
20  
21  
22  
23  
24  
25  
26  
27  
28  
29  
30  
31  
32  
33  
34  
35  
36  
37  
38  
39  
40  
41  
42  
43  
44  
45  
46  
47  
48  
49  
50  
51  
52  
53  
54  
55  
56  
57  
58  
59  
60



73x28mm (300 x 300 DPI)

Peer Review Only

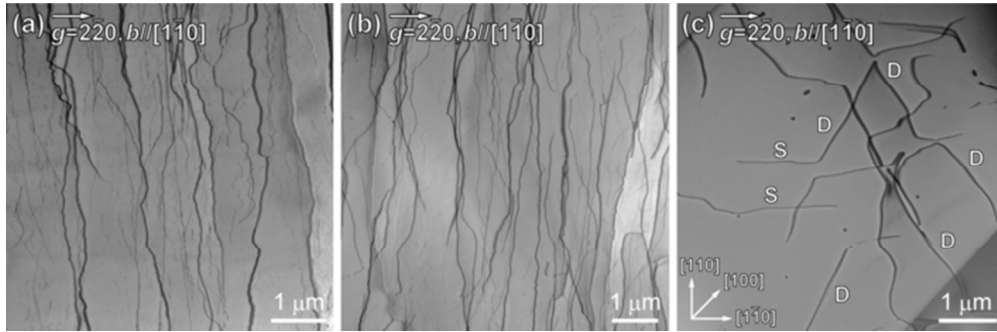


74x29mm (300 x 300 DPI)

Peer Review Only

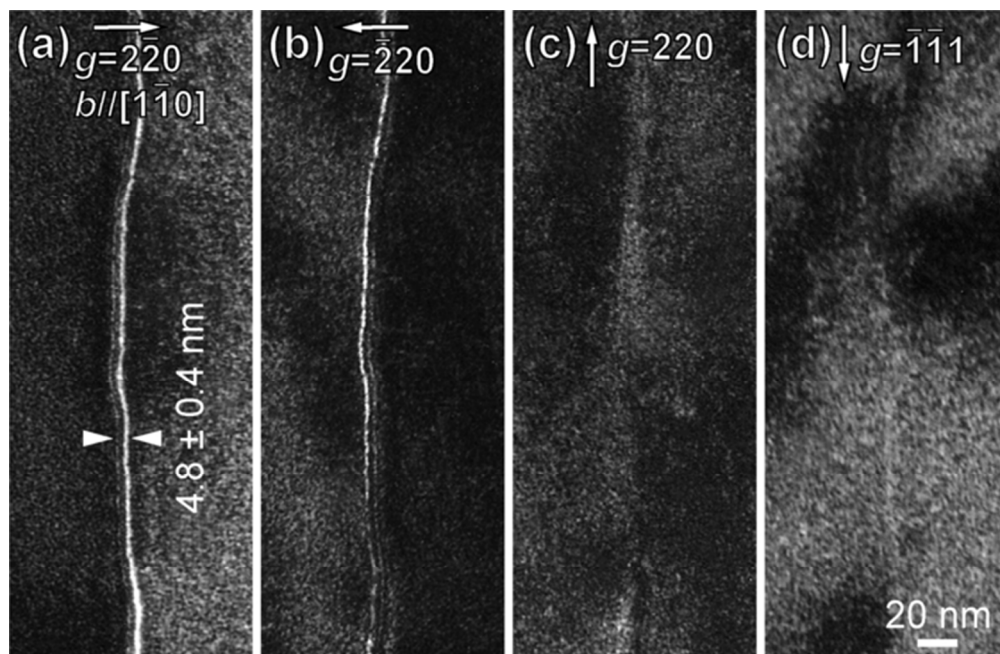
1  
2  
3  
4  
5  
6  
7  
8  
9  
10  
11  
12  
13  
14  
15  
16  
17  
18  
19  
20  
21  
22  
23  
24  
25  
26  
27  
28  
29  
30  
31  
32  
33  
34  
35  
36  
37  
38  
39  
40  
41  
42  
43  
44  
45  
46  
47  
48  
49  
50  
51  
52  
53  
54  
55  
56  
57  
58  
59  
60

1  
2  
3  
4  
5  
6  
7  
8  
9  
10  
11  
12  
13  
14  
15  
16  
17  
18  
19  
20  
21  
22  
23  
24  
25  
26  
27  
28  
29  
30  
31  
32  
33  
34  
35  
36  
37  
38  
39  
40  
41  
42  
43  
44  
45  
46  
47  
48  
49  
50  
51  
52  
53  
54  
55  
56  
57  
58  
59  
60



59x19mm (300 x 300 DPI)

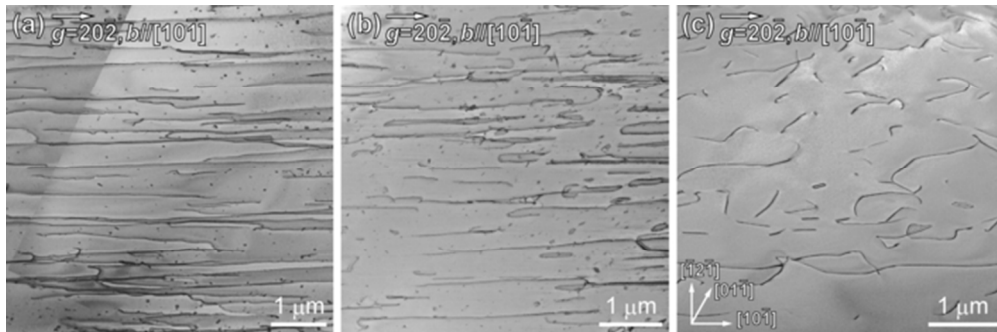
Peer Review Only



59x38mm (300 x 300 DPI)

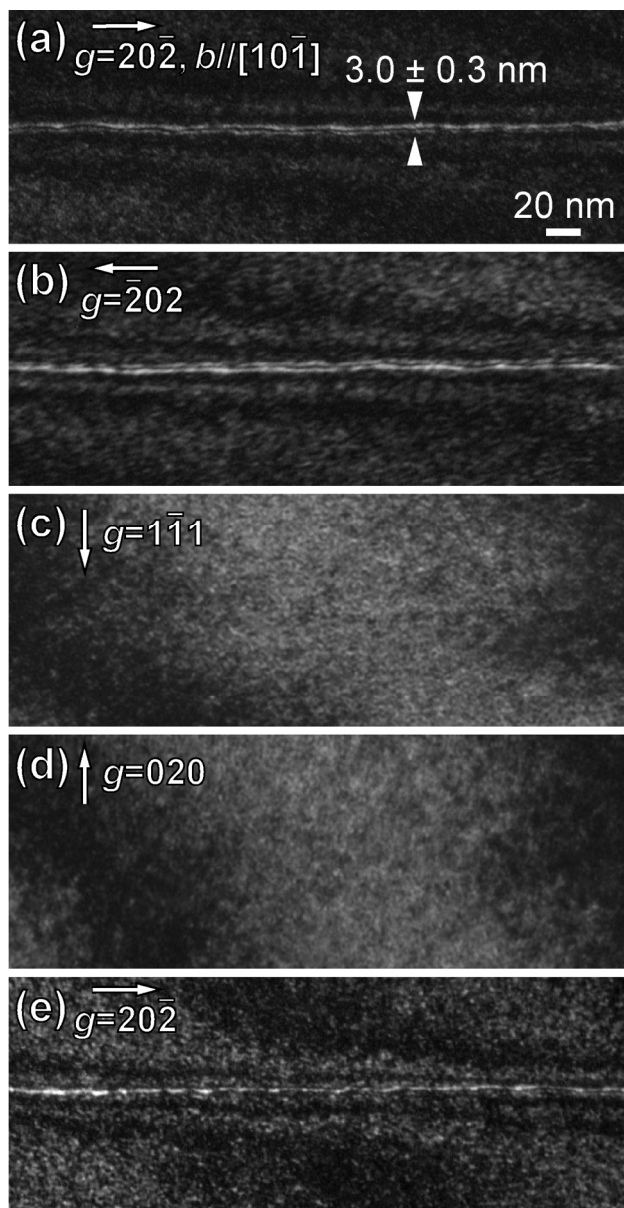


1  
2  
3  
4  
5  
6  
7  
8  
9  
10  
11  
12  
13  
14  
15  
16  
17  
18  
19  
20  
21  
22  
23  
24  
25  
26  
27  
28  
29  
30  
31  
32  
33  
34  
35  
36  
37  
38  
39  
40  
41  
42  
43  
44  
45  
46  
47  
48  
49  
50  
51  
52  
53  
54  
55  
56  
57  
58  
59  
60



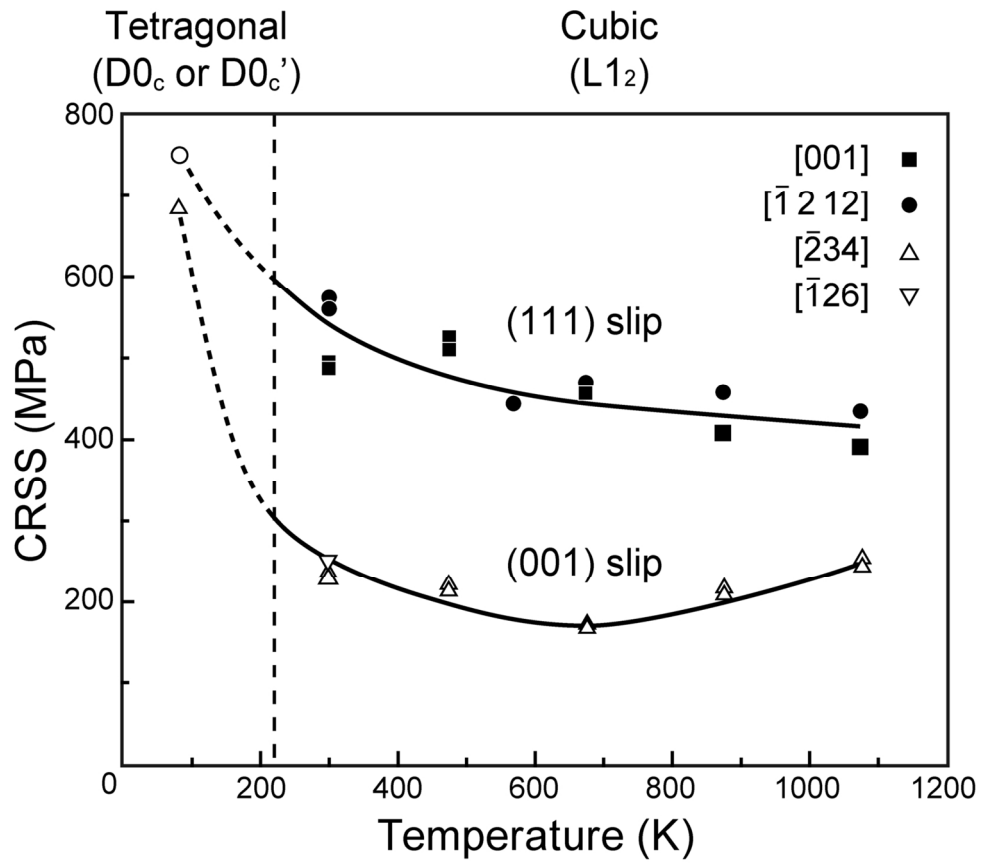
59x19mm (300 x 300 DPI)

Peer Review Only



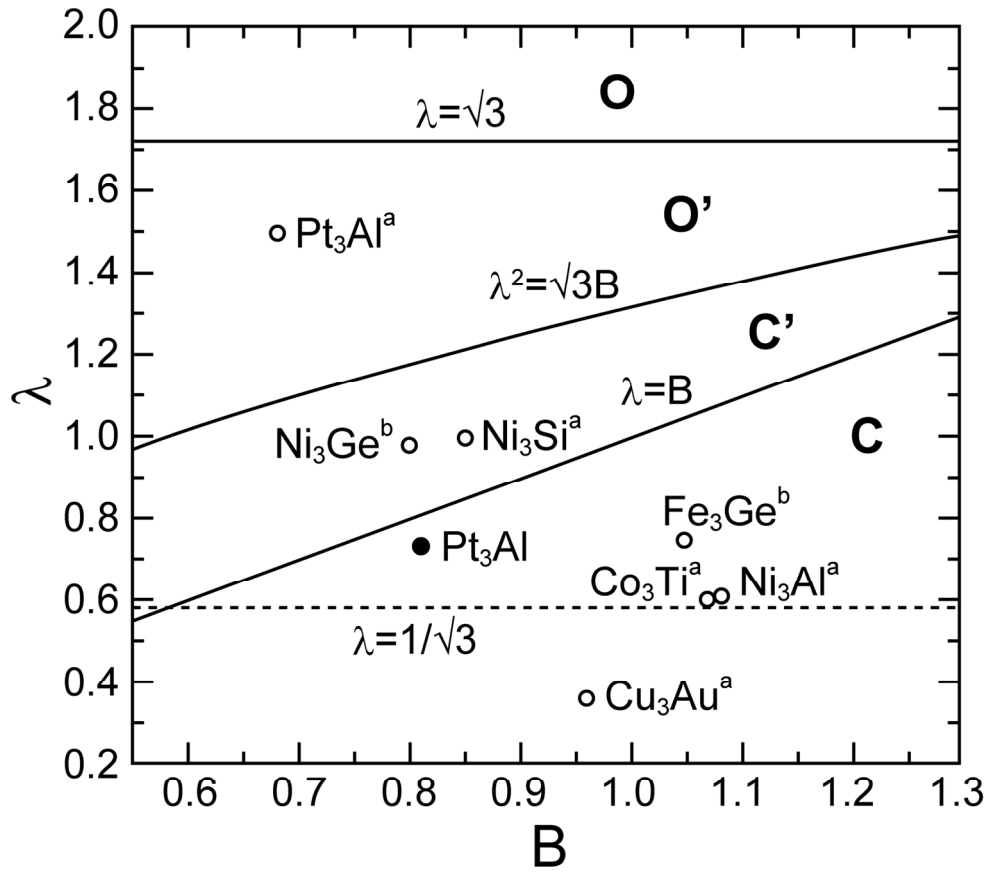
115x223mm (300 x 300 DPI)

1  
2  
3  
4  
5  
6  
7  
8  
9  
10  
11  
12  
13  
14  
15  
16  
17  
18  
19  
20  
21  
22  
23  
24  
25  
26  
27  
28  
29  
30  
31  
32  
33  
34  
35  
36  
37  
38  
39  
40  
41  
42  
43  
44  
45  
46  
47  
48  
49  
50  
51  
52  
53  
54  
55  
56  
57  
58  
59  
60



71x61mm (600 x 600 DPI)

Manuscript Only



77x69mm (600 x 600 DPI)